

# Chemical Binding States of Carbon Atoms Migrated in Tungsten Coating Layer Exposed to JT-60U Divertor Plasmas

Masakatsu FUKUMOTO, Tomohide NAKANO, Yoshio UEDA<sup>1)</sup> and Kiyoshi ITAMI

*Japan Atomic Energy Agency, Naka, Ibaraki 311-0193, Japan*

<sup>1)</sup> *Graduate School of Engineering, Osaka University, Suita, Osaka 565-0871, Japan*

(Received 5 July 2013 / Accepted 13 September 2013)

Carbon migration in the tungsten coating layer exposed to JT-60U divertor plasmas has been investigated by analysis of chemical binding states of the carbon atoms. More than 1% of carbon atoms were accumulated as graphitic carbon, amorphous carbon and/or carbon-deuterium bonds. This concentration was more than five orders of magnitude higher than the solubility of carbon atoms in tungsten lattice. Up to 20% of ditungsten carbide ( $W_2C$ ) was also formed in the tungsten coating layer. These findings suggested the following carbon migration mechanism in the tungsten coating layer. The incident carbon migrates along grain boundaries and defects such as pores over the depth which is evaluated by the carbon diffusion coefficient in tungsten lattice. The carbon atoms trapped on grain surface penetrate and diffuse in the grains. The carbon atoms exceeded the solubility of carbon atoms in tungsten lattice chemically bind to tungsten atoms and form  $W_2C$ .

© 2013 The Japan Society of Plasma Science and Nuclear Fusion Research

Keywords: tungsten, carbon, tritium retention, mixed material, JT-60U

DOI: 10.1585/pfr.8.1405159

## 1. Introduction

In-vessel tritium inventory is one of the most crucial issues for future deuterium-tritium (DT) fusion devices. Carbon based materials such as graphite and carbon fiber composites (CFCs) have been widely used as plasma facing components (PFCs) due to its advantages of low radiation in the core plasma, high thermal conductivity, and high thermal shock resistance [1]. However, since carbon is chemically eroded by hydrogen isotope plasma exposure in addition to physical erosion, an erosion rate of carbon PFCs is high even at a low incident hydrogen ion energy (<100 eV) compared with other candidate materials such as tungsten. The eroded carbon atoms are transported in the plasma and are deposited with hydrogen isotopes on surfaces of armor tiles and remote areas such as tile gaps [2]. The codeposits, especially deposited on the remote area, increase in-vessel tritium inventory since they are difficult to be removed by plasma irradiation.

Tungsten is planned to be used for the PFCs in future fusion devices such as International Thermonuclear Experimental Reactor (ITER) to reduce in-vessel tritium inventory. The advantages of tungsten are low hydrogen solubility, low sputtering yield, and high melting point. Before the DT operation phase in ITER, the CFC monoblocks at the divertor targets will be replaced with tungsten monoblocks [3]. In addition, it is under consideration that the beryllium first wall tiles are replaced by tungsten coated tiles before the later DT operation phase. Even though the carbon tiles are removed from the vacuum vessel, carbon ions should

still remain in the plasma [4]. These carbon ions are injected to the tungsten coating layer together with tritium ions.

Tungsten coated tiles exposed to the divertor plasmas in JT-60U and ASDEX Upgrade have been analyzed to investigate the effects of carbon on hydrogen retention. In these tokamaks, tungsten-coated tiles were installed to investigate feasibility of tungsten as the PFCs, for example, tungsten accumulation and its suppression in the core plasmas [5, 6], tungsten migration [7, 8] and in-vessel deuterium retention [9]. After experimental campaigns, a part of the tungsten-coated tiles were taken out and deuterium and carbon accumulation in the tungsten coating layers were investigated [10–12]. Carbon was injected and accumulated in the tungsten coating layer [10, 11]. It was found that the carbon migration depth was longer than that of thermal diffusion length in tungsten lattice [12]. The deuterium atoms were predominantly trapped by the migrated carbon atoms in the tungsten coating layer [12]. This suggests that migration of carbon atoms plays an important role for hydrogen retention in the tungsten coating layer. In order to investigate the carbon migration mechanisms, in this study, depth profiles of chemical binding states of carbon atoms accumulated in the tungsten coating layer exposed to JT-60U divertor plasmas were analyzed.

## 2. Experimental

### 2.1 Exposure of the tungsten coated tiles

Figure 1 shows a cross sectional view of a tungsten-coated tile. Rhenium and tungsten multi-layer with a thick-

author's e-mail: fukumoto.masakatsu@jaea.go.jp

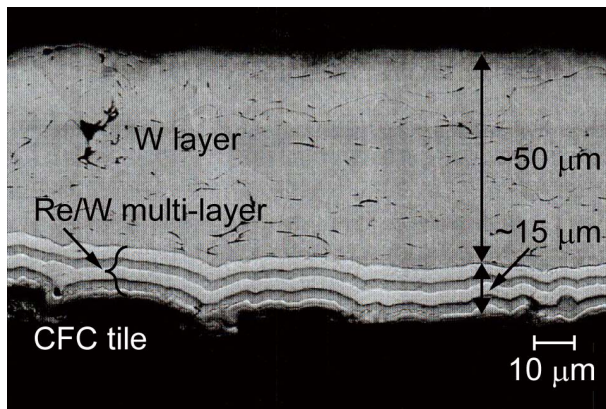


Fig. 1 A cross sectional view of a tungsten-coated tile.

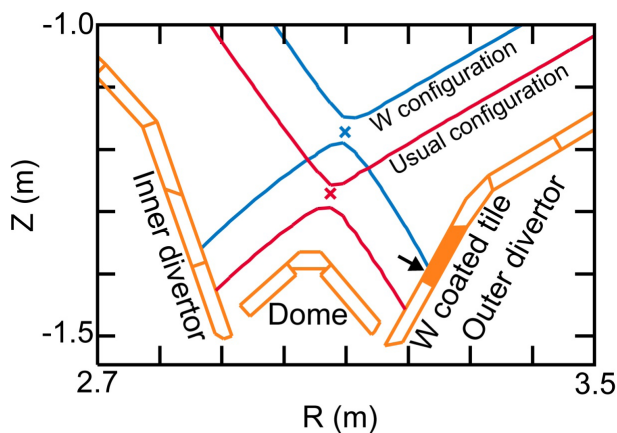


Fig. 2 Poloidal cross-section of the JT-60U divertor region. The two curves indicate the typical positions of the separatrix for the magnetic configurations of a usual and a tungsten accumulation experiment. The filled tile shows the tungsten coated CFC tile. The arrow indicates the analysis point.

ness of  $\sim 15 \mu\text{m}$  was deposited by physical vapor deposition (PVD) on the CFC tiles to reduce carbon diffusion from the CFC substrate [13]. Tungsten with a thickness of  $\sim 50 \mu\text{m}$  was coated by vacuum plasma sputtering (VPS) on the rhenium/tungsten multi-layer.

In JT-60U, 12 tungsten-coated tiles were installed at the upper part of the outer divertor plates before the 2003-2004 experimental campaign as shown in Fig. 2. The outer divertor plate is erosion dominant. In the 2003-2004 experimental campaign, 978 discharges were performed with an outer striking point positioned on the lower part of the divertor plates (the usual configuration), whereas 25 discharges were performed on the upper part of the divertor plates (the tungsten configuration), as shown in Fig. 2. The incident ion fluence during the experimental campaign, evaluated by the Langmuir probe array, was of the order of  $10^{25}$  ions/m<sup>2</sup>. The electron temperature measured by the Langmuir probe array was up to 50 eV. The maximum surface temperature during the plasma discharges

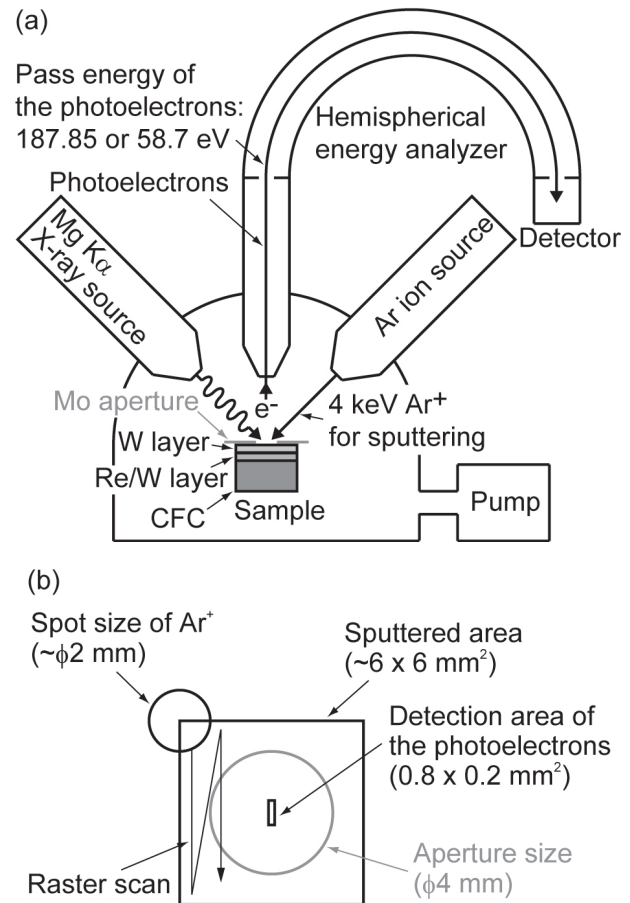


Fig. 3 (a) Schematic view of X-ray photoelectron spectroscopy (XPS) device for the analysis of the chemical binding state of the carbon atoms in the tungsten coating layer. The photoelectrons illuminated from the sample are shown by  $e^-$ . (b) A top view of the sample with the molybdenum aperture. The argon ion beam focused to a diameter of  $\sim 2$  mm is raster-scanned over an area of  $6 \times 6 \text{ mm}^2$  to sputter the tungsten coating layer evenly.

with the strike point positioned on the tungsten coated tiles was  $\sim 700$  K. This temperature was evaluated by finite element methods (FEM) based on the tile temperature measured with thermocouples embedded at  $\sim 6$  mm below the CFC tile surface installed on the same poloidal position. Before air ventilation, 105 shots of hydrogen discharges with hydrogen neutral beam injection (NBI) heating were performed to remove the tritium retained at the tile surfaces.

## 2.2 Post mortem analysis

After the experimental campaign, two tungsten-coated CFC tiles were taken out from JT-60U for the present post mortem tile analysis. Accumulated elements and chemical binding states of carbon atoms were analyzed with X-ray photoelectron spectroscopy (XPS). A sample with a size of about  $8 \times 8 \times 1 \text{ mm}^3$  was cut out from the position at  $\sim 10$  mm from the lower tile edge at which the ion fluence was the highest for the tungsten coated tile. Figure 3(a)

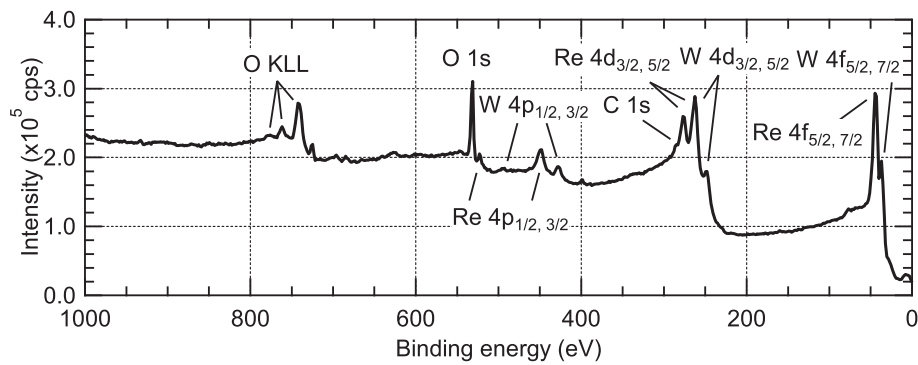


Fig. 4 Low resolution photoelectron spectra detected at  $\sim 20$  nm in depth. Background is not subtracted. Oxygen and rhenium are detected in addition to carbon. The O KLL indicates the Auger electrons emitted from the L-shell by relaxation of the electron from the L-shell to K-shell.

shows schematic view of the XPS device used in this study, and Fig. 3 (b) shows a top view of the sample with the molybdenum aperture. The X-ray generated from an Mg  $K\alpha$  X-ray source was focused to the area of  $0.8 \times 0.2$  mm<sup>2</sup> on the surface of the tungsten coating layer placed in the chamber at a pressure below  $5 \times 10^{-7}$  Pa. The photoelectrons emitted from the surface passed through a hemispherical energy analyzer and were detected with a channel electron multiplier. After the photoelectron spectrum was measured, an argon ion beam at a beam energy of 4 keV was injected through an aperture with a 4 mm in diameter to sputter the tungsten coating layer in order to investigate next deeper layer. As shown in Fig. 3 (b), the argon ion beam focused to about 2 mm in diameter on the sample surface was raster-scanned over an area of  $6 \times 6$  mm<sup>2</sup> to sputter the surface evenly. The XPS measurement and the sputtering by argon ion beam were repeated to measure the depth profile of carbon, oxygen, and rhenium down to 2.5  $\mu$ m. Prior to the measurement, the surface with a thickness of about 20 nm was sputtered to reduce air contamination. The depth profile of oxygen in unexposed tungsten coating layer was also measured to compare with plasma exposed one. Prior to the measurements, the unexposed one was heated at 1373 K for 10 min in a separated vacuum chamber to remove residual gas. The depth of the sputtered crater was measured by a surface profilometer. Note that binding energies of photoelectron spectra were calibrated with the Au  $4f_{7/2}$  photoelectron spectrum with a peak at 84.0 eV taken from a clean surface of a gold sample.

A low resolution photoelectron spectrum was taken in the binding energy range between 1.6 and 1000 eV, as shown in Fig. 4. The photoelectron energy through the hemispherical energy analyzer (pass energy) was set at 187.85 eV and the photoelectrons were measured every 1.6 eV (energy step).

High resolution C 1s and W 4f photoelectron spectra were measured, as shown in Figs. 5 (a) and (b), respectively. The measured energy ranged from 275 to 295 eV for the C 1s spectrum and varied from 25 to 40 eV for the W 4f

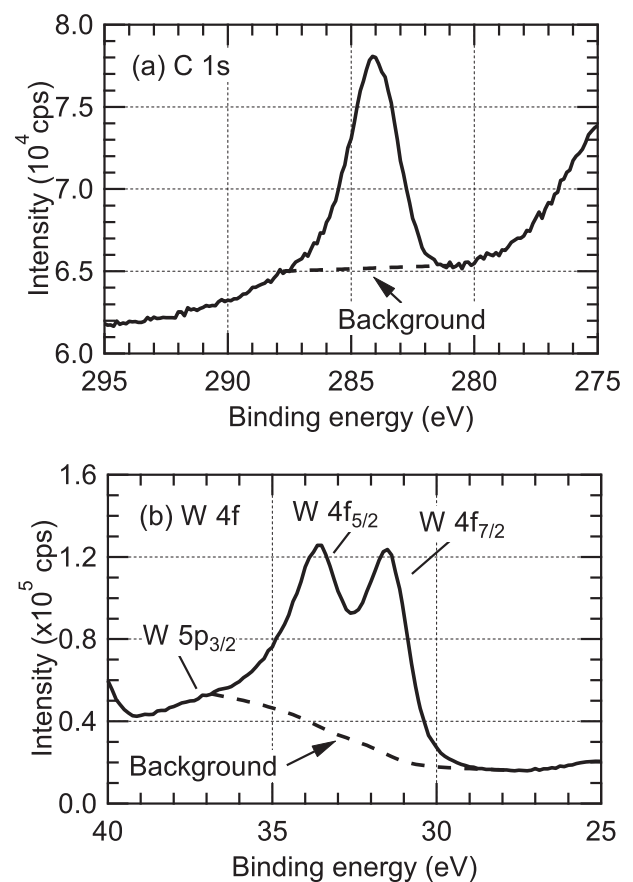


Fig. 5 High resolution photoelectron spectra for (a) C 1s and (b) W 4f detected at  $\sim 0.6$   $\mu$ m in depth. The backgrounds are shown by the broken lines. The W  $5p_{3/2}$  photoelectron spectrum is overlapped with the W  $4f_{5/2}$  one.

spectrum. The pass energies and energy steps for both photoelectrons were set to be 58.7 and 0.125 eV, respectively. High resolution spectra emitted from the impurities, oxygen and rhenium, detected from the low resolution spectra were also measured, as shown in Fig. 6. The measured energy ranged from 524 to 540 eV for the O 1s spectrum and

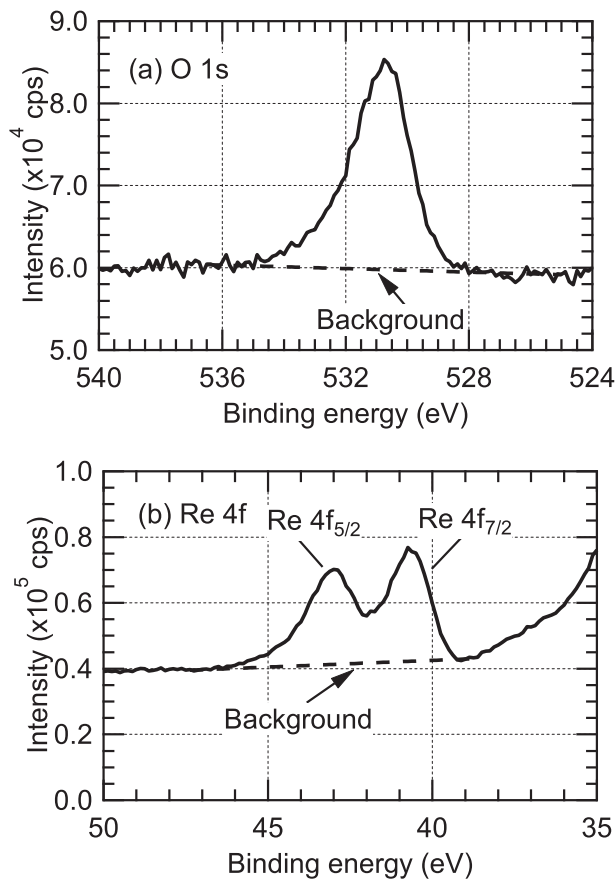


Fig. 6 High resolution photoelectron spectra for (a) O 1s and (b) Re 4f detected at  $\sim 0.6 \mu\text{m}$  in depth. The backgrounds are shown by the broken lines.

varied from 35 to 50 eV for the Re 4f spectrum. The pass energies and energy steps for both photoelectrons were set to be 58.7 and 0.125 eV, respectively.

### 3. Analysis

The high resolution C 1s spectrum is deconvoluted by Voigt functions to determine chemical binding states of carbon atoms. As shown in Fig. 5 (a), the background of the C 1s spectrum, determined by the Shirley's method [14], is subtracted and the resultant spectrum is shown in Fig. 7. The C 1s spectrum can be fitted by four Voigt functions with the different central energies. This is because four different types of carbon chemical binding states are expected from a tungsten-carbon binary system [15]: graphitic carbon, amorphous carbon, tungsten carbide (WC) and ditungsten carbide ( $\text{W}_2\text{C}$ ). Although carbon-deuterium (C-D) bonds are expected to be formed, these cannot be distinguished from the amorphous carbon, due to the same binding energy [16, 17]. The central energies of the Voigt functions are fixed to the binding energies reported in Ref. [15]. These energies are summarized in Table 1. The full width at half maximum (FWHM) and the ratio of the Lorentzian and Gaussian widths were set to be

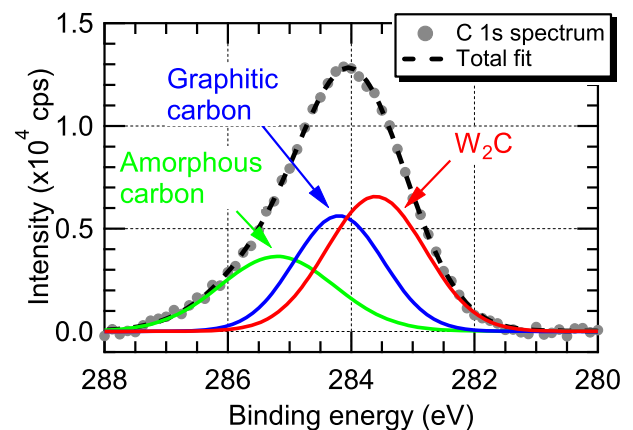


Fig. 7 C 1s spectrum at  $\sim 0.6 \mu\text{m}$  in depth with the best fits for the measured spectrum. The dots show the detected C 1s spectrum after the background subtraction. The three solid lines represent the curves fitted by Voigt functions. The broken line shows total fit of the three Voigt profiles.

Table 1 Binding energies of the electrons at the C 1s electron orbital for the different chemical binding states.

Substance	Binding energy [eV]
Graphitic carbon	284.2
Amorphous carbon	285.2
C-D bounded carbon	285.2
Carbon atoms forming WC	283.1
Carbon atoms forming $\text{W}_2\text{C}$	283.6

free parameters.

Concentrations of carbon atoms with each different binding state over tungsten atoms are determined from an areal ratio of each Voigt profile to W 4f spectrum in consideration of difference of the detection sensitivity between C 1s and W 4f photoelectrons. The background of the W 4f spectrum shown in Fig. 5 (b) is subtracted. The sensitivity factors included in the MultiPak software package [18] are used. Concentrations of oxygen and rhenium atoms over tungsten atoms are also determined by a similar method to the carbon.

### 4. Results

Figure 7 shows the C 1s spectrum taken at  $\sim 0.6 \mu\text{m}$  in depth. Although the measured spectrum is fitted by four Voigt profiles, it can be fitted by the three profiles. From the areal ratio of these Voigt profiles to the W 4f spectrum (Fig. 5 (b)), the concentration of carbon atoms over tungsten atoms are determined to be 15, 8, and 19% for graphitic carbon, amorphous carbon and/or C-D bonds, and carbon atoms forming  $\text{W}_2\text{C}$ , respectively.

Depth profiles of concentrations of carbon atoms with different chemical binding states, determined from the

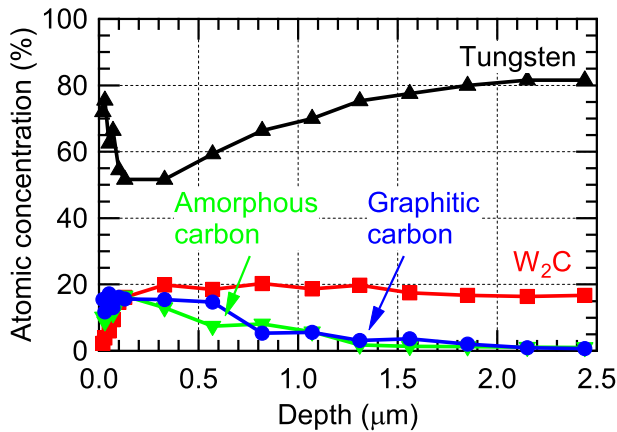


Fig. 8 Depth profiles of concentrations of carbon atoms with different chemical binding states in the tungsten coating.

above method, are shown in Fig. 8. The atomic concentrations are determined with carbon and tungsten although other atoms such as oxygen and rhenium are accumulated in the tungsten coating layer. A concentration of the graphitic carbon is uniform with 15% within  $0.6 \mu\text{m}$  from the surface, and is down to 1% at  $2.5 \mu\text{m}$  in depth. A concentration of the amorphous carbon and/or C-D bounded carbon is uniform at 10–15% within  $0.1 \mu\text{m}$  from the surface. Then it decreases with increasing depth, down to 1%. A concentration of the carbon atoms forming  $\text{W}_2\text{C}$  is 2% at the surface. It increases with depth and saturates to 20% over  $0.3 \mu\text{m}$  in depth.

## 5. Discussion

### 5.1 Carbon migration through the grain boundaries

The concentration of the carbon atoms chemically unbound to the tungsten atoms, i.e. graphitic carbon, amorphous carbon, and/or C-D bound carbon, exceeds the solubility of carbon atoms in tungsten lattice. The solubility of carbon atoms in tungsten lattice extrapolated from the experimental results [19] to 700 K is evaluated to be  $10^{-4}\%$ . However, the concentration of the carbon atoms unbound to the tungsten atoms is more than 1%. This discrepancy indicates possible interpretations that the carbon atoms over the solubility is retained along the grain boundaries and defects such as pores in the present tungsten coating layer.

The carbon migration length in the present tungsten coating layer is much longer than the carbon diffusion length evaluated by the carbon diffusion coefficient in tungsten lattice. Diffusion length,  $l_d$ , in materials is defined as

$$l_d = \sqrt{Dt}. \quad (1)$$

Here,  $D$  ( $\text{m}^2/\text{s}$ ) is the diffusion coefficient and  $t$  (s) is the diffusion time. The carbon diffusion coefficient at 700 K is

evaluated to be up to  $5 \times 10^{-19} \text{m}^2/\text{s}$  from extrapolations of the experimental results [20–23]. With this diffusion coefficient, the carbon diffusion length is evaluated to be up to 70 nm with a surface temperature of the tungsten coating of 700 K during plasma discharge and discharge duration of 8420 s in the 2003–2004 experimental campaign. This diffusion length is more than 40 times shorter than the analyzed depth ( $\sim 2.5 \mu\text{m}$  in depth). Therefore, the present carbon migration length cannot be explained simply by carbon diffusion in tungsten lattice, suggesting another, much faster carbon migration mechanisms in the tungsten coating layer.

Although carbon diffusion coefficients along grain boundaries in VPS-tungsten coating layer have not been determined, diffusion along grain boundaries and defects, in general, is much faster than that through crystal lattice [24]. Therefore, it is probable that the injected carbon atoms and hydrocarbon molecules should migrate along the grain boundaries and defects in the tungsten coating layer. Since the carbon atoms and hydrocarbon molecules which migrated along the grain boundaries would be trapped on the grain surfaces, more than 1% of the carbon atoms unbound to the tungsten atoms were detected.

### 5.2 $\text{W}_2\text{C}$ formation

As shown in Figs. 7 and 8, it is found that  $\text{W}_2\text{C}$  was also formed in the present tungsten coating layer. In the case where carbon atoms penetrate to tungsten grains, carbon atoms exceeded the solubility in tungsten lattice chemically bind to tungsten atoms and form WC or  $\text{W}_2\text{C}$ . Hence, retention of  $\text{W}_2\text{C}$  in the present tungsten coating layer indicates that the carbon atoms trapped on grain surface penetrate to grains through the grain surface and diffuse in the grains, forming  $\text{W}_2\text{C}$ .

Although a concentration of the carbon atoms forming  $\text{W}_2\text{C}$  has the maximum value at 33% in tungsten-carbon binary system, it was saturated at 20% in the present tungsten coating layer. This discrepancy arises from the followings: (i) the carbon migration through grain boundaries and defects is much faster than the carbon diffusion in tungsten grains, and (ii)  $\text{W}_2\text{C}$  is formed only within 70 nm from grain surfaces. Tungsten atoms in the central part of tungsten grains should not be chemically bind to carbon atoms. Hence, additional plasma discharges will grow  $\text{W}_2\text{C}$  formation toward the central part of tungsten grains up to 33% in tungsten coating layer. To confirm this, analysis of a concentration of the carbon atoms forming  $\text{W}_2\text{C}$  in the tungsten coating layer exposed to a longer experimental campaign is in preparation.

### 5.3 Effects of oxygen and rhenium on carbon migration

As shown in Fig. 4, oxygen and rhenium were seen in the present tungsten coating layer. According to the re-

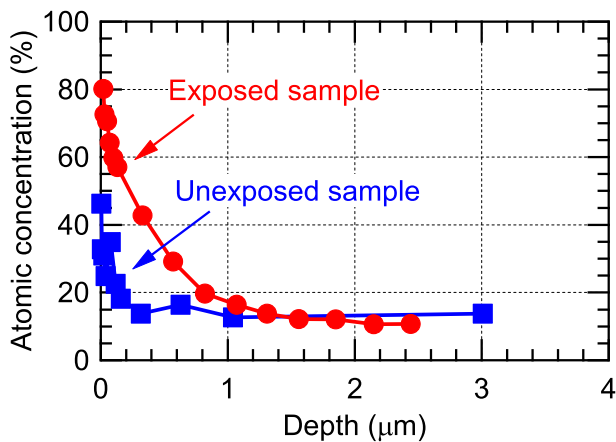


Fig. 9 Depth profiles of concentrations of oxygen atoms in the tungsten coating layer exposed and unexposed to JT-60U divertor plasmas.

port from the manufacturer, concentrations of oxygen and rhenium atoms measured at the time of manufacture were less than 0.1 and 0.01%, respectively, over tungsten atoms. These values are lower than detection limit of XPS (about 1%). This indicates a possibility that the oxygen and rhenium atoms were retained in the present tungsten coating layer during plasma discharges or the tile storage in air after the taking out from the torus.

Since the oxygen atoms originate mainly from atmosphere during the tile storage in air, the effects on the carbon migration would be negligible. Figure 9 shows depth profiles of concentrations of oxygen atoms over tungsten atoms in the tungsten coating layer exposed and unexposed to JT-60U divertor plasmas. The atomic concentrations were determined with oxygen and tungsten. For the unexposed one, the oxygen atoms detected from more than 0.3  $\mu\text{m}$  in depth originate mainly from the residual gas in the XPS device. This indicates for the exposed one that the oxygen atoms at the depth of 1.4  $\mu\text{m}$  or more also originate from the residual gas. Hence, the oxygen atoms within 1.4  $\mu\text{m}$  in depth accumulate during plasma discharge or the tile storage in air after the experimental campaign. In the case that the oxygen is injected during plasma discharges, the incident oxygen atoms would migrate over 1.4  $\mu\text{m}$  in depth such as carbon and deuterium [11, 12]. Hence, the oxygen atoms within 1.4  $\mu\text{m}$  in depth would be accumulated during the tile storage in air after the experimental campaign.

Effects of rhenium on the carbon migration would be also small. Figure 10 shows a depth profile of a concentration of rhenium atoms in the present tungsten coating layer. The atomic concentrations were determined with rhenium and tungsten. Although the rhenium atoms would originate from those in the rhenium/tungsten multi-inter layer [25, 26], the reason why the rhenium atoms retained at the surface of the tungsten coating layer is unclear [26]. The

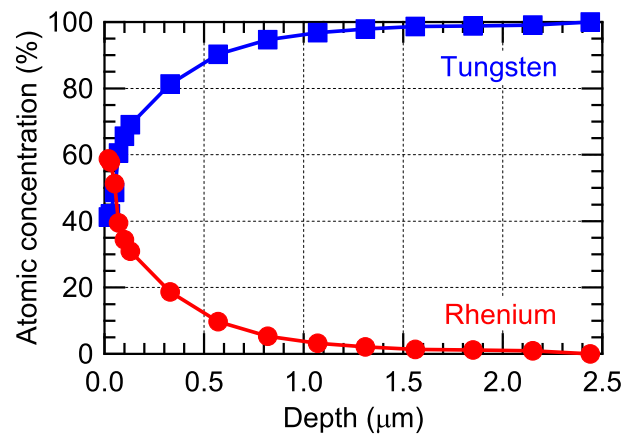


Fig. 10 A depth profile of concentration of rhenium atoms in the tungsten coating layer exposed to JT-60U divertor plasmas.

carbon diffusion coefficient in lattice of tungsten and rhenium alloy increases with the concentration of the rhenium atoms [23]. With the carbon diffusion coefficient evaluated by an extrapolation of the experimental values [23], the carbon atoms injected at initial of the experimental campaign can diffuse up to 0.3  $\mu\text{m}$  in depth in the alloy with rhenium content shown in Fig. 10. Hence, enhancement of diffusion of the carbon atoms in the tungsten coating layer by the rhenium atoms is limited within 0.3  $\mu\text{m}$  in depth.

#### 5.4 Possible carbon migration mechanisms

From the above discussion, we show possible migration mechanisms of the incident carbon in the tungsten coating layer. As shown in Fig. 11 (a), carbon atoms and hydrocarbon molecules inject into the tungsten coating within ion ranges (less than 10 nm in depth). As shown in Fig. 11 (b), the carbon injected near the grain boundaries and pores migrates within  $\sim 2.5 \mu\text{m}$  in depth along grain boundaries and pores. As shown in Fig. 11 (c), the carbon atoms trapped on grain surface penetrate and diffuse in grains. In the case of the hydrocarbon molecules, these dissociate to carbon and hydrogen atoms on grain surfaces and the carbon atoms penetrate and diffuse in the grains. Carbon atoms less than  $\sim 10^{-4}\%$  (solubility of carbon atoms in tungsten lattice at 700 K) solve in grains. The others exceeded the solubility chemically bind to tungsten atoms, forming  $\text{W}_2\text{C}$ . The  $\text{W}_2\text{C}$  is formed within 70 nm from grain boundaries. To confirm the migration mechanisms of the incident carbon, mapping analysis of carbon atoms on the cross-section of the tungsten coating is planned.

Carbon migration through grain boundaries would be enhanced, in particular, in tungsten coating materials. Similar carbon migration mechanisms were reported by Yeh et al. for tungsten thin films produced by magnetron sputtering [27]. They proposed that the carbon atoms penetrated from diamond substrates to the tungsten coating layers mi-

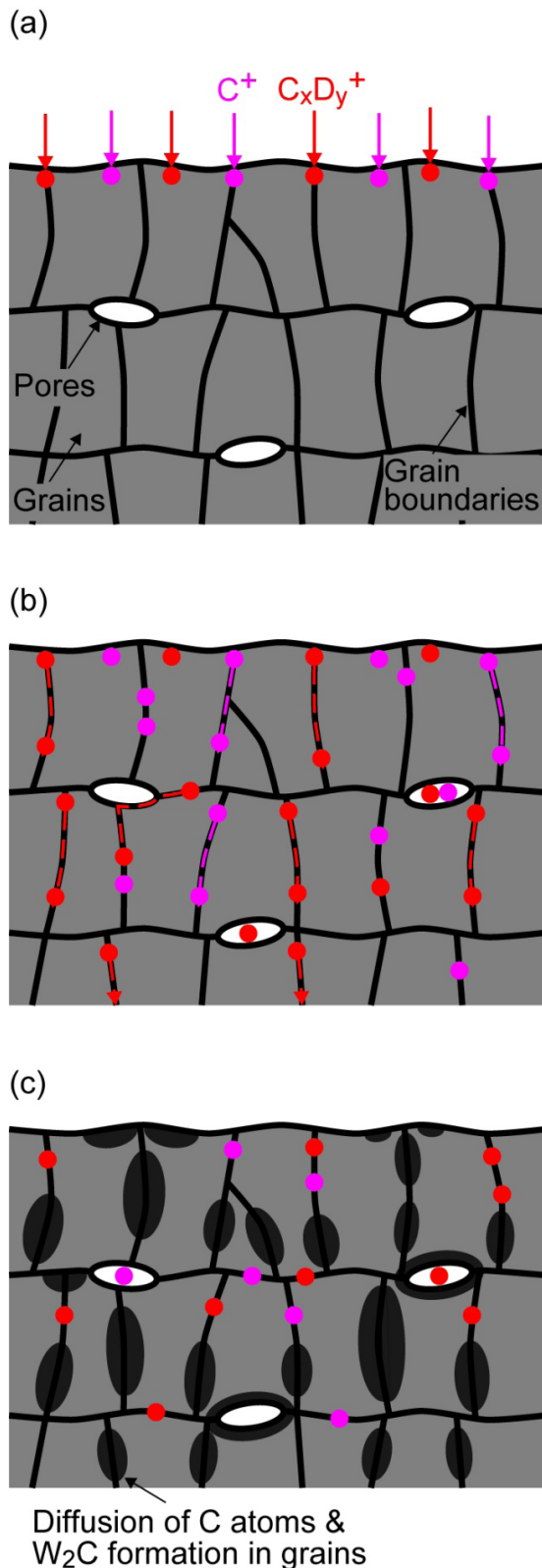


Fig. 11 Possible migration mechanisms of the incident carbon ions in the tungsten coating exposed to JT-60U divertor plasmas. (a) Irradiation of carbon atoms and molecules in the tungsten coating. (b) Migration of carbon along grain boundaries and pores and deposition on the surface of grain boundaries. (c) Penetration and diffusion of carbon atoms in tungsten grains, and chemically binding with tungsten atom and forming  $W_2C$ .

grate through grain boundaries and interstitials, and carbide formation ( $WC$  and  $W_2C$ ) grows from the surface of grain boundaries to inside of the grains. In contrast, preferential migration through grain boundaries is not clearly observed in hot rolled polycrystalline tungsten plates irradiated with carbon and hydrogen ions [28].

One of the possible reasons for the difference of carbon migration between the tungsten coating layer and polycrystalline tungsten plates would be difference of grain-boundary width. The grain-boundary width in the tungsten plates should be narrower than that in the tungsten coating layer since the tungsten plates are hot rolled after sintering of tungsten powder. To prevent the carbon migration through grain boundaries in tungsten coating layer, decrease of the grain-boundary width by some methods such as hot isostatic pressing (HIP) will be effective. This method presses materials isotropically at elevated temperature (a few hundreds of  $^{\circ}C$ ) by an isostatic high pressure gas (a few tens of MPa), and is widely used to reduce the porosity and increase the density of materials.

Suppression of the carbon migration through grain boundaries should be effective to reduce tritium retention in the tungsten coating layer. Tritium retention in the tungsten coating layer increases with the concentration of carbon atoms. This is confirmed by similar depth profiles of deuterium and carbon atoms in the tungsten coating measured by secondary ion mass spectroscopy (SIMS) [11, 12]. This indicates that the injected deuterium atoms are predominantly trapped by carbon atoms accumulated in the tungsten coating layer. Therefore, suppression of carbon migration through grain boundaries should lead to decrease of tritium retention in tungsten coating layer.

## 6. Conclusion

It is found that a concentration of more than 1% of carbon atoms chemically unbound to tungsten atoms, i.e. graphitic carbon, amorphous carbon and/or C-D bound carbon, were retained along the grain boundaries and defects in the tungsten coating layer on the JT-60U outer divertor plates. Concentrations of these carbon atoms exceeded the solubility of carbon atoms in tungsten lattice ( $\sim 10^{-4}\%$ ). A concentration of carbon atoms chemically bound to tungsten atoms, i.e.  $W_2C$ , over tungsten atoms was evaluated to be 20%. The injected carbon atoms were migrated over the depth at a much higher speed expected from the carbon diffusion coefficient in tungsten lattice. From these findings, carbon migration mechanisms are suggested as follows. The incident carbon atoms and hydrocarbon molecules migrate along grain boundaries and defects such as pores over the depth which is evaluated by the carbon diffusion coefficient in tungsten lattice. The carbon atoms trapped on grain surfaces penetrate in grains and diffuse in the grains. The hydrocarbon molecules trapped on grain surfaces would dissociate at grain surfaces and the dissociated carbon atoms penetrate and diffuse in

grains. The carbon atoms exceeded the solubility of carbon atoms in tungsten lattice chemically bind to tungsten atoms, forming  $W_2C$ .

From the results of the present work, simultaneous injection of carbon and tritium ions in a tungsten coating layers in a future DT fusion device leads to increase tritium retention in the tungsten coating layer due to migration of carbon atoms through grain boundaries. Migration of carbon atoms through grain boundaries need to be prevented to reduce tritium retention in tungsten coating layer. This will be achieved by density increase between grains by means of HIP. In order to investigate the crystalline structure of the tungsten coating layer and detailed carbon migration mechanisms, cross-sectional observations with field emission scanning electron microscope (FE-SEM) and transmission electron microscope (TEM) are now to be prepared.

- [1] D. Naujoks, *Plasma-Material Interaction in Controlled Fusion* (Springer-Verlag, Heidelberg) p.213.
- [2] A. Kreter *et al.*, *J. Nucl. Mater.* **390-391**, 38 (2009).
- [3] R.A. Pitts *et al.*, *J. Nucl. Mater.* **438**, S48 (2013).
- [4] S. Brezinsek *et al.*, *J. Nucl. Mater.* **438**, S303 (2013).
- [5] T. Nakano *et al.*, *Nucl. Fusion* **49**, 115024 (2009).
- [6] H. Höhnle *et al.*, *Nucl. Fusion* **51**, 083013 (2011).
- [7] Y. Ueda *et al.*, *J. Nucl. Mater.* **363-365**, 66 (2007).
- [8] Y. Ueda *et al.*, *Nucl. Fusion* **49**, 065027 (2009).
- [9] M. Mayer *et al.*, *J. Nucl. Mater.* **390-391**, 538 (2009).
- [10] K. Sugiyama *et al.*, *Nucl. Fusion* **50**, 035001 (2010).
- [11] M. Fukumoto *et al.*, *J. Plasma Fusion Res. SERIES* **9**, 369 (2010).
- [12] M. Fukumoto *et al.*, *J. Nucl. Mater.* **415**, S705 (2011).
- [13] S. Tamura *et al.*, *J. Nucl. Mater.* **329-333**, 711 (2004).
- [14] D. Shirley, *Phys. Rev. B* **5**, 4709 (1972).
- [15] J. Luthin and Ch. Linsmeier, *Surface Science* **454-456**, 78 (2000).
- [16] E. Igarashi *et al.*, *J. Nucl. Mater.* **363-365**, 910 (2007).
- [17] J. Kovac, *Materials and Technology* **45**, 191 (2011).
- [18] MultiPak, Ver. 6.1A, Physical Electronics, 1999.
- [19] H.J. Goldschmidt and J.A. Brand, *J. Less-Common Metals* **5**, 181 (1963).
- [20] L.N. Aleksandrov *et al.*, *Sov. Powder Metall. Met. Ceram.* **4**, 234 (1964).
- [21] I.I. Kovenski, *Diffusion in BCC Metals*. ASM, p.285 (1965).
- [22] V.Ya. Shchelkonogov *et al.*, *Phys. Met. Metallogr.* **25**, 68 (1968).
- [23] A. Shepela, *J. Less-Common Metals* **26**, 33 (1972).
- [24] H. Mehrer, *Diffusion in Solids* (Springer, Berlin, 2007) p.553.
- [25] H. Maier *et al.*, *Phys. Scr.* **T138**, 014031 (2009).
- [26] V. Philipps *et al.*, *Fusion Eng. Des.* **85**, 1581 (2010).
- [27] J.J. Yeh *et al.*, *Diam. Relat. Mater.* **5**, 1195 (1996).
- [28] Y. Ueda *et al.*, *Fusion Eng. Des.* **81**, 233 (2006).